

**Multiple-time-scale framework for understanding the progression of Parkinson's disease**D. S. Andres,<sup>1,2,3</sup> F. Gomez,<sup>1</sup> F. A. S. Ferrari,<sup>1,4</sup> D. Cerquetti,<sup>2</sup> M. Merello,<sup>2</sup> R. Viana,<sup>4</sup> and R. Stoop<sup>1</sup><sup>1</sup>*Institute of Neuroinformatics, University of Zurich and ETH Zurich, Winterthurerstrasse 190, 8057 Zurich, Switzerland*<sup>2</sup>*Institute for Neurological Research Raul Carrea, Fleni Institute, Buenos Aires, Argentina*<sup>3</sup>*Society in Science, The Branco-Weiss Fellowship, administered by ETH Zurich, Switzerland*<sup>4</sup>*Physics Department, Federal University of Parana, Curitiba, Brazil*

(Received 30 June 2014; published 15 December 2014)

Parkinson's disease is marked by neurodegenerative processes that affect the pattern of discharge of basal ganglia neurons. The main features observed in the parkinsonian globus pallidus pars interna (GPi), a subdomain of the basal ganglia that is involved in the regulation of voluntary movement, are pathologically increased and synchronized neuronal activity. How these changes affect the implemented neuronal code is not well understood. Our experimental temporal structure-function analysis shows that in parkinsonian animals the rate-coding window of GPi neurons needed for the proper performance of voluntary actions is reduced. The model of the GPi network that we develop and discuss here reveals indeed that the size of the rate-coding window shrinks as the network activity increases and is expanded if the coupling strength among the neurons is increased. This leads to the novel interpretation that the pathological neuronal synchronization in Parkinson's disease in the GPi is the result of a collective attempt to counterbalance the shrinking of the rate-coding window due to increased activity in GPi neurons.

DOI: [10.1103/PhysRevE.90.062709](https://doi.org/10.1103/PhysRevE.90.062709)

PACS number(s): 87.10.Vg, 87.15.A–, 82.39.Rt, 05.45.–a

**I. INTRODUCTION**

When 50%–70% of the dopaminergic neurons in the substantia nigra pars compacta have died, the wide spectrum of symptoms characteristic of Parkinson's disease (PD) becomes apparent [1]. The most evident and best-known symptom is a progressive impairment of the ability to execute voluntary motor plans, which severely affects a patient's normal life. At more advanced stages, also cognitive, autonomic, and psychiatric domains are affected, with dementia at the latest stage of the disease [2,3]. A vast body of evidence demonstrates the correlation between these manifestations of PD and pathologic changes in the neuronal activity of the basal ganglia (BG). For a review on this subject, see, e.g., Ref. [4]. Characteristic alterations of the firing behavior of single cells manifest in abnormal temporal firing patterns as well as in changed network behavior [5], the main features being pathologically increased activity and enhanced neuronal synchronization [6]. Local field potential (LFP) recordings evidence the presence of pathologic oscillatory activities throughout the parkinsonian globus pallidus pars interna and externa (GPi and GPe, respectively), the subthalamic nucleus (STN), and the striatum (Str) [7]. Since LFP signals reflect the averaged activity of neuron populations, these pathologic oscillations indicate an enhanced synchronization among these neurons [8]. The enhanced synchronization increases the power of the  $\beta$  band (13–30 Hz) of the firing frequency spectrum, which is currently considered a hallmark of PD [9]. The presently most prominent explanatory framework for the pathophysiology of PD is the so-called rate model. It offers an interpretation of PD based on the overactivity of the output of the BG, in particular of the GPi and of the substantia nigra pars reticulata (SNr) [10,11], based on the BG-thalamo-cortical circuitry exhibited in Fig. 1. The mentioned centers have inhibitory projections to the motor thalamus; their overall effect is antikinetic (impairing voluntary movement). The effect of dopamine, which is diminished or lost in PD, is the

reduction of the antikinetic activity by exerting an excitatory effect over the BG circuit “direct pathway” and an inhibitory one over the “indirect pathway.” GPi is not only the main output center of the BG, it is, moreover, one preferred target for deep brain stimulation (DBS) therapy [12]. In the near future, in-depth knowledge regarding the underlying mechanisms of DBS may lead to a smart brain “pacemaker” [13,14].

Detailed modeling at the level of cellular properties has indicated that DBS can increase the activity at the BG output centers while at the same time regularizing neuronal firing [15]. This would imply that high activity alone might not directly be responsible for the symptoms of the disease [16]. Recently, a new interpretation of parkinsonian akinesia relates the motor impairment in PD to an increased “illegibility” of neuronal information [17]. However, the specific code that BG neurons use to transmit information is yet not well understood, and, moreover, the effects of PD on the neuronal code are unknown. The objective here is to work out what PD's effect on the coding properties of GPi neurons might be. In order to do so, we first concentrate on the full characterization of the firing behavior of the output of a single GPi neuron.

**II. CHARACTERIZATION OF SINGLE NEURONAL FIRING**

Neuronal firing provides typically temporally highly variable, nonstationary, low-frequency noisy (and often relatively short) time series of interspike intervals (ISI). As early as the beginning of the 1980s, it was observed that “using experimental data subject to noise and drift, we find the structure function can be computed to higher accuracy, yet using less data than the correlation function” [18]. For similar reasons, the method was subsequently used in the context of turbulence [19–21]. Later on, the method has been refined in several directions [22], before becoming the standard method in the study of physiological data [22,23]. We use here

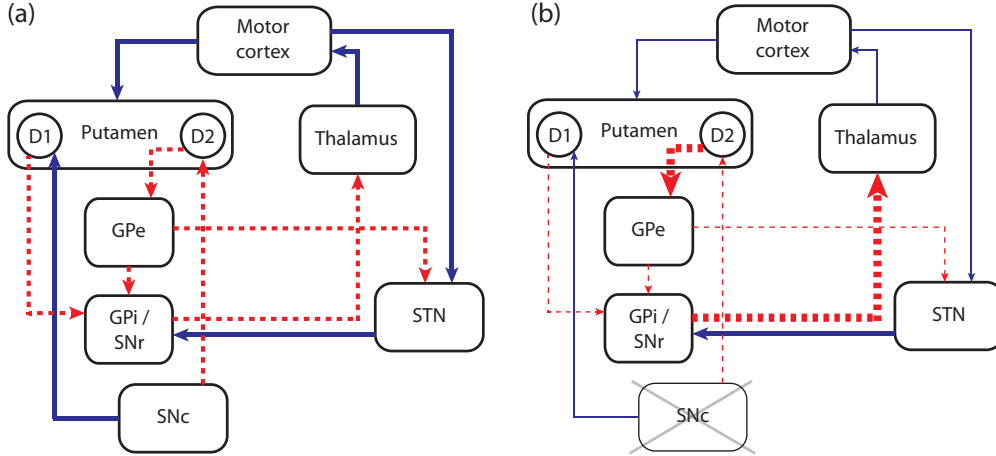


FIG. 1. (Color) Basal ganglia-thalamocortical circuit scheme before (a) and after (b) the emergence of PD. The variation of the arrow thickness from the left to right panel encodes the quantitative changes observed. Blue, excitatory input; red, inhibitory input.

the method in its simplest variant as follows. The structure function of a time series is based on the difference between successive intervals  $I$ ,  $\Delta I_j(\tau) = I(j + \tau) - I(j)$ , where  $j$  is the index of the interval and  $\tau \in \mathbb{N}^+$  is a positive index shift. The structure function  $S_q(\tau)$  of order  $q \in \mathbb{Q}$  is then defined as the average,

$$S_q(\tau) = \langle |\Delta I_j(\tau)|^q \rangle, \quad (1)$$

evaluated over the time series. The approach thus provides information about how correlated interspike intervals are, over some time that corresponds to a time average obtained for an index increase  $\tau$ . Exponent  $q$  provides a magnifying glass for putting more emphasis on “extreme” than on the “normal” cases when performing the average. If one is only interested in the first order ( $q = 1$ ) structure function, the average is numerically feasible as long as the first order of the distribution exists and more involved preprocessing are not needed (normally, first a wavelet analysis of the data is made and the structure function then is performed on the wavelet coefficients of corresponding order). For a simple generating mechanism, scaling properties can be assumed, which implies that we will have a power-law relationship,

$$S_q(\tau) \sim \tau^{\zeta(q)}. \quad (2)$$

The exponent  $\zeta(q)$  then contains the condensed information desired for a distinction of different behaviors of the spike-generating process. Let us exhibit how this happens. For a stationary process with independent increments  $\zeta(q) = 0$ , which expresses that the mean correlation between successive events does not depend on the event index [24]. Monofractal, nonintermittent time series imply  $\zeta'(q) = \text{const}$ , multifractal behavior is characterized by  $\zeta''(q) < 0$  [22,25]. The zero-slope regime of the structure function (as a function of  $\tau$ ) is of particular interest, since it marks the temporal scale across which only random processes are at work. For neuronal signals, this regime precludes coding schemes other than a rate code, and the zero-slope regime can be assimilated to the temporal window of rate-coding. The ability of the first-order structure function to work out these regimes justifies the particular interest we have in it.

### III. DISTINCT NEURONAL CODING REGIMES IN HEALTHY AND PD NEURONS

In a previous work, we showed that the rate-coding window of single GPi neurons is reduced in an animal model of PD [26]. This insight was gained from applying the structure function analysis to neuronal recordings from a group of parkinsonian (6-hydroxydopamine-lesioned) Sprague-Dawley adult rats and comparing the results to those from a healthy control group. The recordings were obtained under two conditions: with animals under deep chloral-hydrate anesthesia and with fully alert animals; both groups were in relaxed, head-restrained conditions. For more detail on our experimental work, the reader is invited to consult Ref. [27]. For the obtained interspike intervals time series, the structure functions of increasing order were calculated. Since for  $q \leq 6$  the results show a mild dependence on the order  $q$  only, we will therefore restrain the reported results to order one. In the temporal structure function of the majority of the neurons studied, at least two major regimes were evident. The first regime, starting at small values of  $\tau$ , shows an ascending behavior that terminates abruptly at breakpoint  $\tau_1$  (vertical lines in Fig. 3). This regime characterizes the small-scale correlations within the data. The regime is followed by an essentially flat region that is at the focus of our attention, as this flat region represents the rate-coding window of neuronal activity. In the PD group at all alertness levels, this second regime was substantially reduced. The next-following regime (if identifiable) basically encodes long-term memory processes and is mostly ascending. For Fig. 3, smoothing averaging over five consecutive data points from our modeling approach (see below) was applied; for essentially equivalent experimental animal data, see Ref. [26].

Similar results could, alternatively, be obtained through the (first-order) correlation function; the emergence of  $\tau_1$ , which is one essential ingredient to our analysis, is, however, enhanced by using the structure function framework. Regarding the cases exhibited in Fig. 3, the value of  $\tau_1$  in case I is clearly corroborated. Already in case II, a value of  $\tau_1$  becomes more difficult to extract and for the PD cases III and IV, this is virtually impossible (cf. the corresponding autocorrelation

function in our Supplemental Material [28]). In the structure function approach, exhibited in Fig. 3, we have no difficulties in determining an approximate value of  $\tau_1$ .

The main changes observed in the temporal structure function of parkinsonian GPi neurons can be summarized as follows: At all alertness levels, PD neurons have a shortened rate-coding window, a prolonged regime I (with a higher  $\tau_1$ ) under anesthesia, and an increasing structure function for almost every  $\tau$  at full alertness, where the rate-coding window almost disappears. To understand these results on the neuronal level, we investigated a simplified model of the parkinson and the healthy GPi.

#### IV. A MODEL OF THE PARKINSONIAN AND NONPARKINSONIAN GPi

To obtain insight into the origins of this changed behavior, we simulated the behavior using an abstract model of the GPi, composed of a ring of coupled neurons [26]. The specific network architecture can be seen in Fig. 2.

In the ring, 101 Rulkov neurons were implemented, where each neuron follows the dynamical equations [29],

$$x_{i,n+1} = f(x_{i,n}, y_{i,n} + \beta_{i,n}), \quad (3)$$

$$y_{i,n+1} = y_{i,n} - \mu(x_{i,n} + 1) + \mu\sigma + \mu\sigma_{i,n}, \quad (4)$$

where the index  $n$  indicates the iteration step, and where function  $f$  is given by

$$f(x_n, y) = \begin{cases} \alpha/(1-x_n) + y, & x_n \leq 0 \\ \alpha + y, & 0 < x_n < \alpha + y \wedge x_{n-1} \leq 0 \\ -1, & x_n \geq \alpha + y \vee x_{n-1} > 0. \end{cases} \quad (5)$$

In this model,  $x_n$  represents the membrane voltage of the  $i$ th neuron at discrete time  $t = 0, 1, 2, \dots, n$  and  $y_{i,n}$  is the slow recovery or adaptation variable. External input (from STN or Str) is modeled by the current

$$\sigma = \sigma_u + I_c, \quad (6)$$

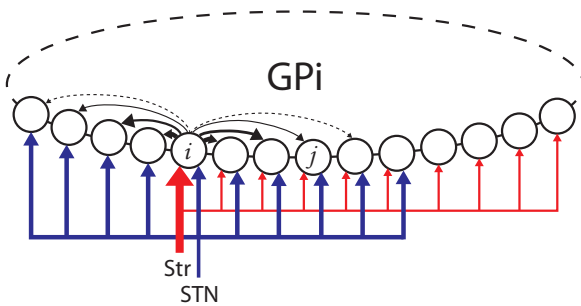


FIG. 2. (Color) Model architecture. GPi neurons are arranged in a ring and diffusively coupled to each other ( $n = 101$ , circles). The Str afference to the GPi (inhibitory) is modeled with 101 axons, each of which connected to one GPi neuron with a high synaptic weight ( $w_{\text{Str-GPi-I}} = 0.9$ ) and to 9 GPi neurons with a lower weight ( $w_{\text{Str-GPi-II}} = 0.01$ ). STN input, excitatory, is represented by 101 axons, each of which produces 10 collaterals to adjacent GPi neurons with the same synaptic weight ( $w_{\text{STN-GPi}} = 0.1$ ). Small-range interactions are modeled by diffusive coupling among GPi cells.

where  $\sigma_u$  represents the initial excitability of each isolated neuron and  $I_c$  models the input to the cell. Rulkov neurons are very general and versatile to model virtually any neuronal firing behavior (cf. Refs. [30,31], where Rulkov neurons have been explicitly related to measured neuronal behavior).

STN and Str inputs to GPi are modeled as excitatory and inhibitory inputs, respectively, and the spatial distribution of both inputs is close to the available histological data [32]: Excitatory input to the GPi is mediated by 101 STN axons, each of which sends collaterals to 10 neighboring cells using identical synaptic weights ( $w_{\text{STN-GPi}} = 0.1$ ). Inhibitory input to the GPi is mediated by 101 Str axons producing also 10 collaterals each (Fig. 2): one central connection to a GPi neuron with a high synaptic weight ( $w_{\text{Str-GPi-I}} = 0.9$ ) and 9 connections to adjacent cells with a lower weight ( $w_{\text{Str-GPi-II}} = 0.01$ ). For every neuron, the parameter values  $\alpha = 4.5$  and  $\mu = 0.001$  are used. The dynamical coupling from each neuron  $i$  to its neighbors has the form ([29], where we set  $\beta^e$  and  $\sigma^e$  to 1)

$$\beta_{i,n} = g_{ji}\beta^e(x_{j,n} - x_{i,n}), \quad (7)$$

$$\sigma_{i,n} = g_{ji}\sigma^e(x_{j,n} - x_{i,n}), \quad (8)$$

where in our case the coupling constants  $g_{ji}$  depend in a power-law decay fashion on the distance between the neurons measured along the ring structure,

$$g_{ji} = \frac{D}{|(i-j)|^2}. \quad (9)$$

In neural tissues, diffusive coupling is well-known and also referred to as ephaptic coupling; see Ref. [33]. Inputs  $I_c$  were modeled by uniformly distributed random numbers from the unit interval, multiplied by amplitudes  $A_e$  and  $A_i$  for excitatory and for inhibitory input, respectively. To account for variability in initial neuronal excitation,  $\sigma_u$  was drawn uniformly from [0.05,0.15]. To test the intrinsic behavior of the network, the use of an uncorrelated input seems to be indicated, since, in this way, the specific signatures produced in the signal by the emergent behavior of the network itself can unfold without competing effects.

#### V. RESULTS OF MODEL SIMULATIONS

After a transient phase, the system was iterated for 180 000 time steps and spikes were extracted to obtain ISI time series. After a suitable choice of the few parameters inherent in the model, our simulation reproduced the experimental animal data very well (Fig. 3, comparable to the experimental data in Ref. [26]). The classical model of PD [10] bases the distinction between the healthy and the PD case on distinct excitatory and inhibitory input levels, which we extended for the distinction between anesthetized and alert conditions [26]. Whereas the anesthetized condition was modeled by  $A_i = -1.2$  (-24.5) and  $A_e = 1.5$  (25), the alert condition was modeled by  $A_i = -1.5$  (-48.5) and  $A_e = 2$  (50) [for control (PD), respectively]. This led to  $|\frac{A_i}{A_e}|$  ratios of 0.8 (0.98) (anesthesia) and 0.75 (0.97) (alertness) [control (PD), respectively]. To reproduce the temporal structures for the four experimental groups studied (control and PD groups, under deep anesthesia and at full alertness; Fig. 3, panels I-IV), in addition to the classical

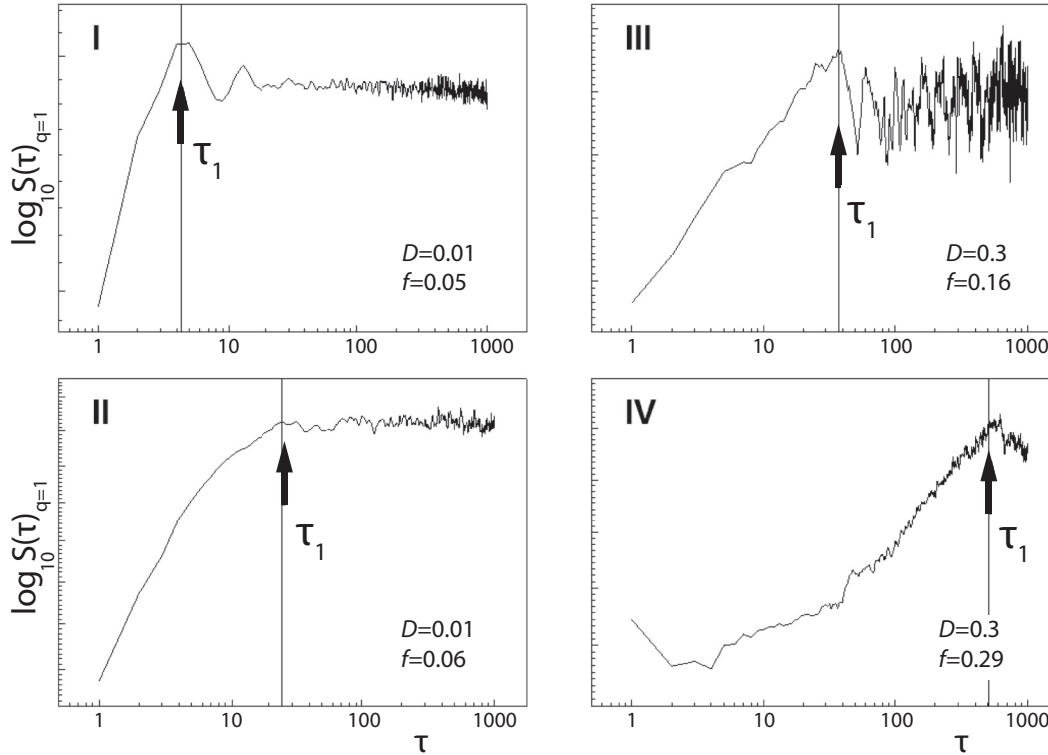


FIG. 3. Order-1 structure functions of the four modeled groups representing our neuronal classes of behavior. (I, II) Control group, deep anesthesia, and alert condition, respectively; (III, IV) PD, deep anesthesia, and alert condition, respectively. With alertness, for groups I to III, the breakpoint moves to the right and finally disappears in group IV, and a progressive reduction of the zero-slope scale range is observed, indicating a loss of the rate-coding capability for PD neurons.  $f$  indicates the average frequency connected with the index interval  $\tau$  and  $1/f$  the corresponding “typical” time scale (in the model in units of iterations).

model (see Sec. VI for more details) we also had to use distinct diffusion constants ( $D = 0.3$  in the PD versus  $D = 0.01$  in the healthy case). The network activity was calculated as the mean across the network of the number of spikes divided by the number of iterations. Figure 4 shows the network activity as a function of the input level, for different coupling strengths and at different  $|A_i/A_c|$  ratios. As can be expected, with higher input levels, the network activity increases before it saturates. This also holds with respect to higher levels of  $D$ , since higher levels of coupling induce higher levels of  $g_{ji}$  [cf. Eq. (9)]. Compared to healthy conditions, at PD input conditions the network saturates at higher external input and at higher activity levels.

The degree of synchronization of neuronal activity, a hallmark of PD, was calculated as the mean [34,35]

$$M_n = \frac{1}{N} \sum_{i=1}^n x_i, \quad (10)$$

where  $x_i$  is the fast variable corresponding to the  $n$  neurons of the network. In the case of weak neuronal coupling, the mean fluctuates irregularly, because the firing of individual neurons is noncoherent. Conversely, if the neurons start to fire coherently and become synchronized, then regular oscillations of comparatively large amplitudes of  $M_n$  emerge. To characterize this, for each simulation a synchronization measure  $A_m$  was calculated as the difference between the

highest and lowest values of  $M_n$ . As a tendency, increasing  $D$  enhances neuronal synchronization [Fig. 5(b)]. When  $A_m > 1.0$ , we considered a network synchronized, which we then take as the hallmark for a simulated PD network state.

To obtain a network-representative breakpoint  $\tau_1$ , we averaged the individual structure functions over the network. The obtained averaged structure function  $\bar{S}$  shows behaviors similar to the structure functions of the individual neurons of the respective classes. To evaluate  $\tau_1$  we calculated the first derivative of the averaged structure function,  $\bar{S}'$ , and defined  $\tau_1$  as the smallest  $\tau$  for which  $\bar{S}' < 0$  for three consecutive  $\tau$ .

In our four experimental groups, the breakpoint  $\tau_1$  moves to the right from the control case under deep anesthesia (group I), to the control case at full alertness (group II), and the PD case under anesthesia (group III), and is highest in the PD case at full alertness (group IV). In this last group an increasing temporal structure function at almost every scale is observed, and the zero-slope window essentially disappears. This marks the progressive reduction of the zero-slope scale range, indicating a loss of the rate-coding properties in PD neurons, which are even more deteriorated under the effect of full alertness.

With our modeling framework, we successfully reproduced this behavior; it is worthwhile emphasizing that the distinct behaviors are the emergent consequences of the different global network conditions, expressed at the level of single cells, but are not the intrinsic properties of single neurons.

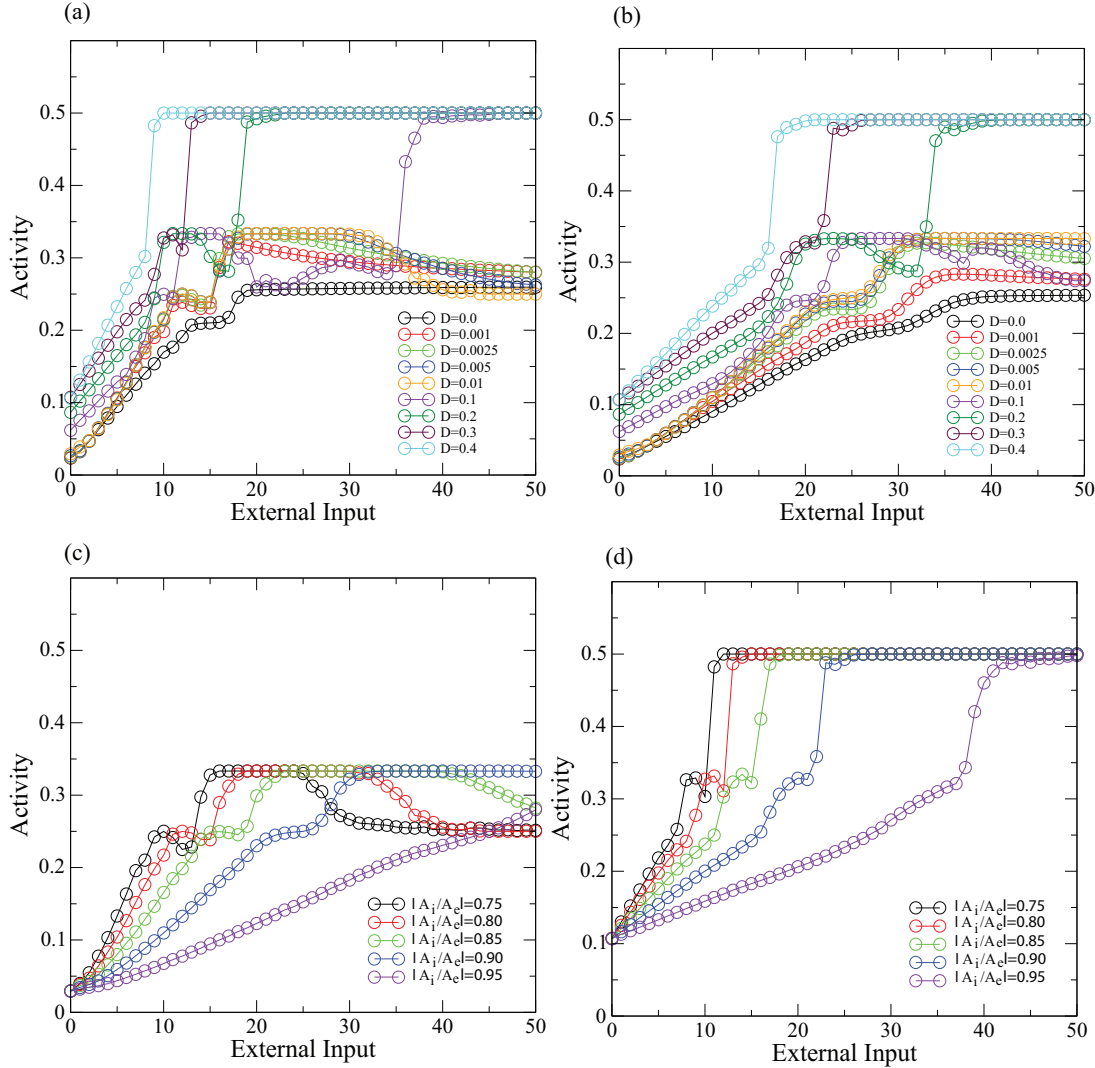


FIG. 4. (Color) Average network activity: Growing external input entrains increased activity (a) healthy conditions [ $A_i/A_e = 0.8$ , external input  $< 5$ , typically  $\in (1.5, 2)$ ], (b) toward parkinsonian conditions [ $A_i/A_e = 0.9$ , external input  $\in (25, 50)$ ], (c) healthy conditions [ $D = 0.01$ , typically  $D < 0.1$ , external input  $< 5$ , typically  $\in (1.5, 2)$ ], (d) toward parkinsonian conditions [ $D = 0.3$ , typically  $D \in (0.3, 0.5)$ , external input  $\in (25, 50)$ ].

Breakpoint  $\tau_1$  limits the size of the rate-coding window from the left-hand side (a higher  $\tau_1$  implies a shorter rate-coding window). Understanding the variables that determine its position can help gaining new insights into the network changes that parkinsonian neurons account for. In particular, we focused on the dependence of  $\tau_1$  on two main network variables: the coupling strength  $D$  and the mean network activity (Fig. 5).

**VI. DISCUSSION AND INTERPRETATION OF RESULTS**

The traditional rate-mode explanatory framework for the pathophysiology of PD (Fig. 1) offers an interpretation of PD based on the overactivity of the output structures of the BG, namely the GPi and the SNr [10,11]. Since these output centers are connected with an inhibitory projection to the motor thalamus, their overall effect is considered to be antikinetic (impairing voluntary movement). This antikinetic activity is stimulated through the indirect pathway of the

BG, and inhibited through the direct pathway (therefore considered antikinetic and prokinetic, respectively). The effect of dopamine, which is diminished or lost in PD, is to reduce the antikinetic activity by exerting a stimulatory effect over the direct pathway and an inhibitory one over the indirect pathway of the BG circuit. The dopamine loss liberates the spontaneous activity of the GPi. Although there is substantial agreement about the increased activity of the GPi in PD [36,37], a clear causal relationship with the symptoms of the disease has not been established. Accepting the premises of the rate model, the GPi's overactivity could explain bradykinesia. Some major controversies, however, arise between the rate model and several electrophysiological findings obtained during functional neurosurgery in human patients [38]. In the first place, there is evidence showing that high-frequency DBS of the GPi further increases its activity [39–41]. DBS, moreover, provides a benefit for PD patients when applied to different parts of the BG-thalamo-cortical circuitry: a reduction of the symptoms has been observed applying the

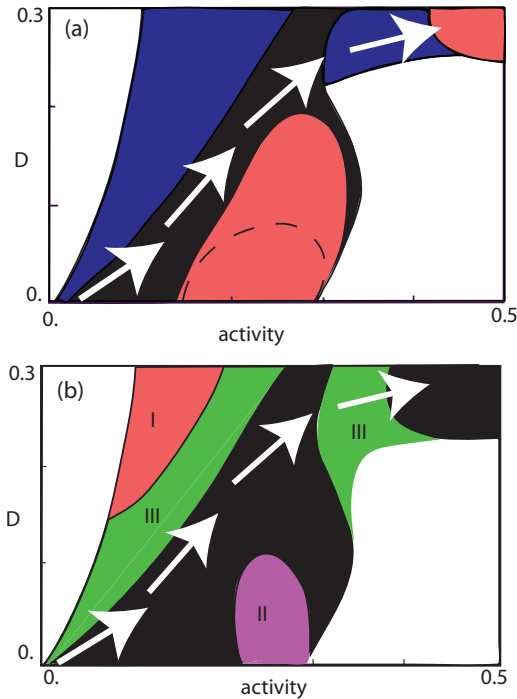


FIG. 5. (Color) White arrows: Suggested development of PD. The parameters (activity,  $D$ ) provide a coherent qualitative description of the situation, although they are not fully independent. (a)  $\tau_1$  evaluated as a function of the network activity and  $D$  (at  $|A_i/A_e| = 0.95$ ). Blue ( $\tau_1 < 100$ ) and black ( $100 < \tau_1 < 500$ ) indicate viable rate-coding windows. Red: Vanishing rate-coding window ( $\tau_1 > 500$ ). In the course of PD increased activity, to escape a coding window collapse,  $D$  must increase as well. From  $|A_i/A_e| = 0.90$  to  $|A_i/A_e| = 0.95$ , the red area increases from the dashed boundary to the final one. (b) Network synchronization as a function of the network activity and on  $D$  (at  $|A_i/A_e| = 0.9$ ). The situation remains essentially unchanged for  $|A_i/A_e|$  in  $(0.8, 0.95)$ . White, unaccessible regime; black, viably unsynchronized ( $A_m < 1$ ). Regime I, highly synchronized across all of the interval ( $A_m > 2$ ); Regime II, very strong synchronization at  $|A_i/A_e| = 0.8$ , subject to a decrease toward  $|A_i/A_e| = 0.95$  (from  $A_m \approx 4$  to  $A_m = 1.5$ ); Regime III, synchronized across the whole interval ( $1 < A_m < 2$ ). This regime is likely to trigger the typical PD synchronization phenomena.

stimulation to the GPi, the GPe, the STN, motor Thalamus, premotor cortex, and even the zona incerta [42–46]. DBS of the GPi can, moreover, successfully treat hypokinetic PD as well as hyperkinetic movement disorders (dystonia), which according to the rate model are based on oppositional mechanisms.

Our modeling approach suggests that as the GPi network activity increases with the higher input levels present in PD, the length of the rate-coding window progressively shortens and that an appropriate increase in the diffusive coupling  $D$  might postpone this effect [Fig. 5(a)]. The price to be paid for this, however, would be the danger of enhanced network synchronization. In fact, the neuronal activity of the BG in PD is known to be pathologically synchronized [9]. Experimental evidence about pathological synchronization in the parkinsonian BG comes mainly from LFP studies that

show an increased power in specific frequency ranges in the BG with PD [47]. Both pharmacological anteparkinsonian treatment and DBS therapy have been shown to normalize the LFP profiles [48,49]. These facts, unfortunately, failed to provide any insight about the organization of neuronal firing in the time-domain.

The results indicate that different time scales may be at work in the healthy and PD GPi. This speaks in favor of a multiple-scale rather than of a scale-free temporal organization of neuronal firing, implying that the transmission of information might be favored in or confined to a limited time-range. As we have seen, PD deteriorates these temporal scales. The high activity induced by the disease (exacerbated *in vivo* at full alertness) generate a temporal structure where virtually all the scales are positively correlated. As a consequence, in PD, temporally independent stimuli could no longer be transmitted in a long time-window, making PD neurons extremely sensitive to any spurious input. At the different scales, different mechanisms are likely to be relevant. At small time scales, the behavior seems to be more strongly influenced by local interactions, modeled in our approach by diffusive coupling. Experimental evidence supports that the coupling between adjacent PD Str neurons is pathologically increased [50,51]. It is not far stretched to expect that a similar characterization also holds for the parkinsonian GPi. Up to now, the consequences of an increased coupling regarding information coding have not been investigated. We demonstrate that the length of the rate-coding window in GPi neurons (measured by means of  $\tau_1$  only), depends qualitatively inversely on activity and directly on the coupling strength  $D$ . At activities characteristic for PD, an increased coupling strength may allow GPi neurons to maintain a temporal structure resembling a normal one only at input levels much higher than those observed in the healthy condition. The price to be paid is that of increased neuronal synchronization, accompanied by the well-known abnormal oscillations of parkinsonian neurons. When in PD the limits of the compensatory mechanism are reached by pathologically high activity, GPi neurons are left with a temporal structure growing for almost every scale, which then prohibits largely a rate-coding of information.

These insights into a potential scheme underlying the effects observed in PD emerge from a simple network model that was tuned toward the reproduction of the electrophysiological properties of the basal ganglia under chronic dopamine depletion. Although based on real GPi histology, we deal here with a simplified one-dimensional model. The mammalian GPi has a 3D structure; therefore, a comparison of topological indicators (number of connections, distribution, etc.) can on this level only be of qualitative nature. The developed model reproduces the animal model experiments well, to some extent even reflecting what is found in human PD patients. If a direct relationship between these frequencies to the frequencies of the tremor often shown by PD patients could be made, this would clearly be of interest. However, we would expect such a relationship to be rather complicated, as the transduction from GPi frequencies to frequencies observed on the movement level is far from being trivial, and one needs to be extremely cautious when making comparisons between these cases and human PD. First of all, the discharge frequencies of neurons of the GPi in PD patients depend generally on the state of

activity during which the measurements are taken, and they vary from individual to individual [52]. Second, a distinction needs to be made between the frequencies of discharge of single neurons (such as is done in our modeling) and LFP frequencies. Because the LFP is influenced not only by the frequency of discharge of single cells but also by the (lower) frequency of collective bursting, the LFP power spectrum peak is typically lower than the frequency of discharge of single cells, the latter being around 60–100 Hz [48]. Normally, the LFP peak is found within the  $\beta$  frequency band (13–30 Hz), but we deal also in this respect with considerable variation, even under similar conditions [53]. Under conditions of immobility, the peak value of the distribution has been reported to lie around 20 Hz [54].

For matching the model-obtained frequencies with the generally accepted values observed in human PD, the time step corresponding to one iteration of the Rulkov map [Eqs. (3)–(5)] can be adjusted in an optimal way, the freedom being limited by the fact that all experimental conditions will be affected by such a manipulation in the same manner. Considering a time step equal to 5 ms per iteration, the single-cell frequency of the four groups shown in Fig. 4 would be for the control group 10 Hz (under anesthesia) and 12 Hz (alert), respectively; and for the PD group 32 Hz (under anesthesia) and 58 Hz

(alert). Using this time step, the model would yield a power spectrum peak of the mean field, to be compared to the LFP in humans, around 38 Hz for the PD group. This is in reasonable correspondence with the human data outlined above (58 Hz versus 60–100 Hz for single-cell frequency and 38 Hz versus 13–30 Hz for the spectrum peaks). Most importantly, with this time step, the characteristic bursting of single neurons is faithfully reproduced, as well as the characteristic sizes of the rate-coding windows. This seems to permit the conclusion that, at the level of electrophysiological (emergent) properties, our model provides a reliable reproduction of the biological processes at work in PD.

#### ACKNOWLEDGMENTS

We thank the technical personnel at the Institute of Neuroinformatics, ETH and UZH, Zürich, Switzerland, and at the laboratories of the Center for Applied Neurological Research, Fleni Institute, Buenos Aires, Argentina. The work at the Federal University of Parana, Curitiba, Brazil, was made possible by financial support from the Brazilian government agencies CNPq and CAPES. F.G. and R.S. acknowledge SNF grant 20020-147010/1.

- 
- [1] K. Wirdefeldt, H.-O. Adami, P. Cole, D. Trichopoulos, and J. Mandel, *Eur. J. Epidemiol.* **26**, 1 (2011).
- [2] A. Schrag, *J. Neurol.* **251**, 795 (2005).
- [3] The Guideline Development Group, *Parkinsons Disease: National Clinical Guideline for Diagnosis and Management in Primary and Secondary Care* (Royal College of Physicians, London, UK, 2006).
- [4] A. Galvan and T. Wichmann, *Clin. Neurophysiol.* **119**, 1459 (2008).
- [5] J. A. Obeso *et al.*, *Trends Neurosci.* **23**, S8 (2000).
- [6] M. Filion and L. Tremblay, *Brain Res.* **547**, 142 (1991).
- [7] P. Gatev, O. Darbin, and T. Wichmann, *Mov. Disord.* **21**, 1566 (2006).
- [8] C. Hammond, H. Bergman, and P. Brown, *Trends Neurosci.* **30**, 357 (2007).
- [9] A. A. Kühn *et al.*, *J. Neurosci.* **28**, 6165 (2008).
- [10] R. L. Albin, A. Young, and J. B. Penny, *Trends Neurosci.* **12**, 366 (1989).
- [11] M. R. DeLong, *Trends Neurosci.* **13**, 281 (1990).
- [12] M. C. Rodriguez-Oroz *et al.*, *Brain* **128**, 2240 (2005).
- [13] C. Hauptmann *et al.*, *J. Neural Eng.* **6**, 066003 (2009).
- [14] J. Buhlmann, L. Hofmann, T. A. Tass, and C. Hauptmann, *Front. Neuroeng.* **4**, 15 (2011).
- [15] M. J. Birdno, S. E. Cooper, A. R. Rezai, and W. M. Grill, *J. Neurophysiol.* **98**, 1675 (2007).
- [16] J. E. Rubin and D. Terman, *J. Comput. Neurosci.* **16**, 211 (2004).
- [17] O. Darbin, D. Dees, A. Martino, E. Adams, and D. Naritoku, *BioMed Res. Int.* **2013**, 742671 (2013).
- [18] E. O. Schuls-DuBois and I. Rehberg, *Appl. Phys.* **24**, 323 (1981).
- [19] R. Benzi, S. Ciliberto, R. Tripicciono, C. Baudet, F. Massaioli, and S. Succi, *Phys. Rev. E* **48**, R29 (1993).
- [20] U. Frisch, *Turbulence, The Legacy of A. N. Kolmogorov* (Cambridge University Press, Cambridge, 1996).
- [21] G. P. Romano, R. A. Antonia, and T. Zhou, *Exp. Fluids* **27**, 368 (1999).
- [22] J. W. Kantelhardt, S. A. Zschiegner, E. Koscielny-Bunde, S. Havlin, A. Bunde, and H. E. Stanley, *Physica A* **316**, 87 (2002).
- [23] P. C. Ivanov, L. A. Nunes Amaral, A. L. Goldberger, S. Havlin, M. G. Rosenblum, Z. R. Struzik, and H. E. Stanley, *Nature* **399**, 461 (1999).
- [24] S. I. Vainshtein, K. R. Sreenivasan, R. T. Pierrehumbert, V. Kashyap, and A. Juneja, *Phys. Rev. E* **50**, 1823 (1994).
- [25] J. Peinke, J. Parisi, O. E. Rössler, and R. Stoop, *Encounter with Chaos: Self-Organized Hierarchical Complexity in Semiconductor Experiments* (Springer, Berlin-Heidelberg, 1992).
- [26] D. S. Andres, F. Gomez, D. Cerquetti, M. Merello, and R. Stoop, *Springer CCIS* **438**, 355 (2014).
- [27] D. S. Andres, D. Cerquetti, M. Merello, and R. Stoop, *Front. Neurol.* **5**, 96 (2014).
- [28] See Supplemental Material at <http://link.aps.org/supplemental/10.1103/PhysRevE.90.062709> for elaboration on Fig. 3.
- [29] N. F. Rulkov, *Phys. Rev. E* **65**, 041922 (2002).
- [30] B. Ibarz, J. M. Casado, and M. A. F. Sanjuán, *Phys. Rep.* **501**, 1 (2011).
- [31] S. Martignoli, F. Gomez, and R. Stoop, *Sci. Rep.* **3**, 2676 (2013).
- [32] M. Difiglia and J. A. Rafols, *J. Electron Microsc. Tech.* **10**, 247 (1988).
- [33] C. A. Anastassiou, R. Perin, H. Markram, and C. Koch, *Nature Neurosci.* **14**, 217 (2011).
- [34] Y. Kuramoto, *Chemical Oscillations, Waves, and Turbulence* (Springer, Berlin, 1984).
- [35] F. Mormann, K. Lehnertz, P. David, and C. E. Elger, *Physica D* **144**, 358 (2000).
- [36] Y. Smith, M. D. Bevan, E. Shink, and J. P. Bolam, *Neuroscience* **86**, 353 (1998).

- [37] J. P. Bolam, J. J. Hanley, P. A. C. Booth, and M. D. Bevan, *J. Anat.* **196**, 527 (2000).
- [38] E. B. Montgomery Jr., *Parkinsonism Relat. Disord.* **13**, 455 (2007).
- [39] M. E. Anderson, N. Postupna, and M. Ruffo, *J. Neurophysiol.* **89**, 1150 (2003).
- [40] A. Stefani *et al.*, *Cell Death Dis.* **2**, e154 (2011).
- [41] A. Stefani *et al.*, *Front. Syst. Neurosci.* **5**, 1 (2011).
- [42] E. B. Montgomery Jr. and J. T. Gale, *Neurosci. Biobehav. Rev.* **32**, 388 (2008).
- [43] W. Koller, *Ann. Neurol.* **42**, 292 (1997).
- [44] J. L. Vitek, T. Hashimoto, J. Peoples, M. R. DeLong, and A. E. Bakay, *Mov. Disord.* **19**, 907 (2004).
- [45] J. E. Arle *et al.*, *J. Neurosurg.* **109**, 133 (2008).
- [46] S. Canavero *et al.*, *J. Neurosurg.* **97**, 1208 (2002).
- [47] J. Dostrovsky and H. Bergman, *Brain* **127**, 721 (2004).
- [48] R. Levy, J. O. Dostrovsky, A. E. Lang, E. Sime, W. D. Hutchison, and A. M. Lozano, *J. Neurophysiol.* **86**, 249 (2001).
- [49] M. Weinberger *et al.*, *J. Neurophysiol.* **96**, 3248 (2006).
- [50] C. Cepeda, J. P. Walsh, C. D. Hull, S. G. Howard, N. A. Buchwald, and M. S. Levine, *Synapse* **4**, 229 (1989).
- [51] S. P. Onn and A. A. Grace, *J. Neurophysiol.* **71**, 1917 (1994).
- [52] P. A. Starr, G. M. Rau, V. Davis, W. J. Marks, Jr., J. L. Ostrem, D. Simmons, N. Lindsey, and R. S. Turner, *J. Neurophysiol.* **93**, 3165 (2005).
- [53] B. Wingeier, T. Tchong, M. Miller Koop, B. C. Hill, G. Heit, and H. M. Bronte-Stewart, *Exp. Neurol.* **197**, 244 (2006).
- [54] P. Brown, P. Mazzone, A. Oliviero, M. G. Altibrandi, F. Pilato, P. A. Tonali, and V. Di Lazzaro, *Exp. Neurol.* **188**, 480 (2004).